Resonance production of keV sterile neutrinos in core-collapse supernovae and lepton number diffusion

Vsevolod Syvolap,[1,2] Oleg Ruchayskiy,[1] and Alexey Boyarsky[3]
[1]*Discovery Center, Niels Bohr Institute, Copenhagen University, Blegdamsvej 17, Copenhagen DK-2100, Denmark*
[2]*Taras Shevchenko National Technical University, Kiev 03680, Ukraine*
[3]*Lorentz Institute, Leiden University, Niels Bohrweg 2, Leiden NL-2333 CA, Netherlands*

(Received 20 September 2019; revised 13 June 2022; accepted 16 June 2022; published 19 July 2022)

We investigate how hypothetical particles—sterile neutrinos—can be produced in the interior of exploding supernovae via the resonant conversion of $\bar{\nu}_\mu$ and $\bar{\nu}_\tau$. The novelty of our treatment lies in the proper account of the resulting lepton number diffusion. We compute the yield of sterile neutrinos and find that even after taking into account backreaction, sterile neutrinos can carry out a sizeable fraction of the total energy of the explosion comparable to that of active neutrinos. The production is, however, sensitive to the temperature in the inner supernovae regions, making robust predictions of challenging. In order to understand whether this production affects supernova evolution and can therefore be constrained, detailed simulations including the effects of sterile neutrinos are needed.

DOI: 10.1103/PhysRevD.106.015017

I. INTRODUCTION AND OUTLOOK

Exploding supernovae (SNe) are characterized by high temperatures $T \sim \mathcal{O}(10)$ MeV and high densities of baryons. This makes them unique laboratories that can copiously produce hypothetical feebly interacting particles [1–3], including axions, dark photons, millicharged particles, sterile neutrinos (see, e.g., Refs. [4,5]).

SN medium is not transparent for neutrinos of all flavors, and their dispersion relations change, as compared to the vacuum case $\omega = |k|$ [6]. In the models with *sterile neutrinos* (ν_s)—massive neutral particles, that mix with active neutrinos—this may lead to the enhancement of active-sterile mixing, similarly to the solar MSW effect [7,8]. Feeble interaction of the resulting particles allow them to escape from the interiors of SNe.

The question of sterile neutrino production during supernovae explosion, their effects on explosion, and the stellar nucleosynthesis has been studied in the past [9–28]. These studies mostly concentrated on the mixing of the sterile neutrino with electron flavor, owing to the presence of the significant electron lepton number L_e in the supernova. The production of ν_s from μ and τ flavors has been considered in [17,24,29].[1] These works took into account production via scattering in the constant-density core of the supernova, expecting that the effect should be the strongest there due to the high density of matter and temperature.

The question of production of ν_s, mixed with ν_x has been reanalyzed recently in [30] where it had been noticed that outside the core the resonant MSW-like conversion of $\bar{\nu}_x$ into sterile neutrino ν_s was possible (see also [31]). It was argued in [30] that such a conversion can be quite efficient and can lead to a significant flux of ν_s for mixing angles as small as $\sin^2(2\theta_{\mu,\tau}) \sim 10^{-12}$.

In this work, we re-analyze sterile neutrino production in the course of supernovae explosion, taking into account the backreaction of sterile neutrino emission on the local density of antineutrinos. We demonstrate that

(i) the local density of antineutrinos $\bar{\nu}_x$ in the resonance zone is quickly reduced (the chemical potential $\mu_x \gtrsim T$ is generated), thus slowing the sterile neutrino production,
(ii) the diffusion processes are not efficient enough to restore the population of $\bar{\nu}_x$ in the resonance zone, and
(iii) the exact amount of energy carried by sterile neutrinos is sensitive to the temperature in the inner SN regions. This makes robust predictions of sterile neutrino flux challenging, as these temperatures are not sufficiently constrained.

[1]In what follows we will use the notation ν_x to denote collectively (ν_μ, ν_τ) and $\bar{\nu}_x$ for $(\bar{\nu}_\mu, \bar{\nu}_\tau)$, respectively.

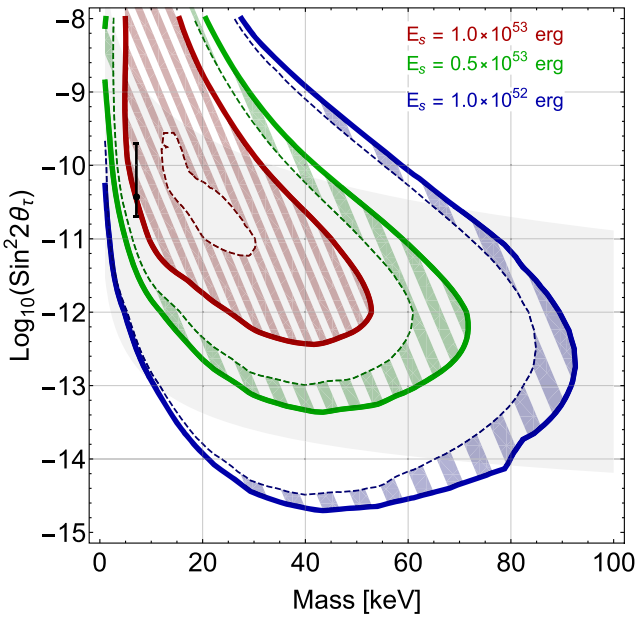

FIG. 1. *Main result*: Energy emitted by sterile neutrinos mixed solely with ν_τ, produced via resonant conversion during the first second after the SN core bounce (thick solid lines). Thinner dashed lines correspond to same emitted energy in the modified model where the temperature is 10% lower. Note, that the contours with energy output $E_s \sim 10^{53}$ erg are only indicative, as we did not include in our treatment the energy loss and cooling due to sterile neutrinos. Although our analysis did not assume that sterile neutrinos are dark matter particles, we overimpose the light gray region to indicate where the correct dark matter abundance of sterile neutrinos can be generated in the *neutrino minimal standard model* (νMSM see Sec. III G). Black dot with error bars corresponds to the 3.5 keV signal of [32,33] interpreted in terms of decays of sterile neutrino dark matter.

As a result the process of sterile neutrino production eventually switches off. Nevertheless, we find that sterile neutrinos can carry out a significant fraction of the total energy of the explosion, comparable with the energy flux of a flavor of active neutrinos. *This constitutes the main result of our paper.*

The structure of the paper and the main points of each section are as follows: Section II lists the formulas that are sufficient to reproduce our results and explains basic ingredients that enter the computations. Details and comments accompanying these formulas are provided in Appendixes. Section III presents our results: we estimate the amount of energy carried away by ν_s, calculate their spectra and evolution of the chemical potential of μ and τ flavors in space and time. Our main results are summarized in Fig. 1. In Sec. IV, we conclude that although sterile neutrino production can be quite efficient, it is difficult to obtain robust constraints on sterile neutrino parameters based on the scarce data we have and that one needs holistic simulations of SN explosions, including sterile neutrinos to see whether too much energy gets carried away through this channel. Appendixes A–D provide background information and additional cross-checks; details of the derivation of the kinetic equation; treatment of the diffusion, etc.

II. SKETCH OF THE COMPUTATIONS

In order to keep the presentation simple and spare readers from technical details, we start by summarizing the main steps of our calculations and basic formulas that would allow one to reproduce our results. Details of the derivation and calculation are provided in Appendix B below.

In order to compute the production of sterile neutrinos we need to solve a *system of coupled equations*

(1) First equation (Eq. (1) below) describes the temporal evolution of the distribution function of sterile neutrinos, based on which one can compute, e.g., sterile neutrino energy flux.
(2) Second equation (Eq. (9) below) governs the evolution of the chemical potential $\mu_x(r,t)$, that describes the backreaction of the sterile neutrino production on the population of active antineutrinos.

The number of ν_s with energy E, resonantly produced by the time t and traveling into the solid angle $d\Omega$ is given by (we assume that $E \approx |\vec{p}|$, i.e., sterile neutrinos are ultrarelativistic):

$$\boxed{\frac{d^2N_s(t,E)}{dE\,d\Omega} = \int_0^t 4\pi R_{\rm res}^2(E) E^2 \bar{f}_x^{\rm out}(t', R_{\rm res}(E), E) P_{x\to s}(E) e^{-R_{\rm fwhm}/\lambda_{\rm mfp}} dt'.} \tag{1}$$

Expression (1) requires several comments. $R_{\rm res}(E)$ is the radius, at which resonance condition is satisfied for antineutrinos with the energy E. Relation $r = R_{\rm res}(E)$ can be inverted to form $E = E_{\rm res}(r)$ and determines the value of the energy of ν_s produced at radius r:

$$E_{\rm res}(r) = \frac{m_s^2}{V_{\rm eff}(r)}. \tag{2}$$

$V_{\rm eff}(r)$ is the *effective potential* of antineutrinos [6]. For the $\bar{\nu}_\mu$:

$$V_{\rm eff}(r) = -\frac{G_F}{\sqrt{2}} N_{\rm b}(Y_n - 2Y_{\nu_e} - 2Y_{\nu_\tau} - 4Y_{\nu_\mu} - 2Y_\mu). \tag{3}$$

Here $Y_i \equiv \frac{N_i - N_{\bar{i}}}{N_{\rm b}}$ is the asymmetry in ith particle ($i = \{n, p, e, \mu, \tau, \nu_e, \nu_\mu, \nu_\tau\}$), $N_{\rm b}$ is the baryons number

density. All these quantities are functions of position, see Appendix A. The effective potential for $\bar{\nu}_\tau$ is obtained by the replacement $\mu \leftrightarrow \tau$ and $\nu_\mu \leftrightarrow \nu_\tau$ in (3). The baryon density $N_{\rm b}$ and asymmetries reach their maximal values in the SN core. Therefore, the energy, entering (1) has a minimal value and the spectrum of emitted sterile neutrinos is cut at low energies.

Initial values of asymmetries Y_i we use in the SN model (see Appendix A) are such, that the potential (3) is *negative*, meaning that the resonance occurs for antineutrinos. Moreover, we found that the potential will not change its sign during the production phase and hence we do not consider any equation for neutrinos conversion.

Numerically, the resonance energy (2) is given by

$$E_{\rm res} \sim 9\ {\rm MeV} \cdot \left(\frac{m_s}{10\ {\rm keV}}\right)^2 \cdot \frac{\rho_B}{3\times 10^{14}\ {\rm g/cm^3}}, \quad (4)$$

where we used for estimate $Y_e = 0.3$, $Y_{\nu_e} = 0.1$ and $Y_\mu = Y_{\nu_\mu} = Y_{\nu_\mu} = 0$.

The transition probability $P_{x\to s}$ is defined as:

$$P_{x\to s} = 1 - \exp\left[-\frac{\pi^2}{2}\frac{R_{\rm fwhm}}{L_{\rm osc}}\right], \quad (5)$$

where $R_{\rm fwhm}$ is the width of the resonance region,

$$R_{\rm fwhm} = \frac{2\sin 2\theta_0}{\left|\frac{\partial \log V_{\rm eff}^{\rm res}}{\partial r}\right|}, \quad (6)$$

(derivative of $V_{\rm eff}$ is evaluated at $r = R_{\rm res}$) and $L_{\rm osc}$ is the oscillation length at the resonance

$$L_{\rm osc} = \frac{2\pi}{|V_{\rm eff}^{\rm res}|\sin 2\theta_0}. \quad (7)$$

The angle θ_0 is the vacuum active-sterile neutrino mixing and all equations are derived for $\theta_0 \ll 1$. The resonance is effective when $R_{\rm fwhm} \gtrsim L_{\rm osc}$, this ratio is $\propto \sin^2(2\theta_0)$.

The distribution function $\bar{f}_x^{\rm out}$ describes *outgoing* antineutrinos at the radius $r = R_{\rm res}(E)$. This function has the *equilibrium* form

$$\bar{f}_x(t,r,E) = \frac{1}{(2\pi)^3}\frac{1}{\exp[\frac{E+\mu_x(r,t)}{T(r)}]+1}. \quad (8)$$

The evolution of the antineutrino population is fully encoded in the chemical potential $\mu_x(r,t)$, we do not take into account temperature evolution during the first second of explosion.

Factor $e^{-R_{\rm fwhm}/\lambda_{\rm mfp}}$ where $\lambda_{\rm mfp}$ is the mean free path of $\bar{\nu}_x$, streaming radially outwards in the resonance region, accounts for the *neutrino damping* [34], see Sec. III F below.

For the distribution (8) the relation between the chemical potential and the asymmetry Y_x is defined as:

$$Y_x = \frac{1}{N_{\rm b}}\left(\frac{\mu_x T^2}{6} + \frac{\mu_x^3}{6\pi^2}\right) \quad (9)$$

and the evolution of Y_x is given by the equation

$$\boxed{\frac{\partial Y_x(r,t)}{\partial t} = \frac{\pi}{6}\frac{N_{\rm b}(r)}{G_F^2 r^2}\frac{\partial}{\partial r}\left(\frac{r^2}{N_{\rm b}(r)}\frac{\partial \mu_x(r,t)}{\partial r}\right) + \frac{\pi}{N_{\rm b}(r)}E_{\rm res}^2(r,t)\bar{f}_x(E_{\rm res}(r),r,t)P_{x\to s}(E_{\rm res}(r),r,t)\frac{dE_{\rm res}}{dr}(r,t),} \quad (10)$$

where the first term describes the diffusion of the lepton number and the second term—the change of lepton asymmetry due to the conversion of antineutrinos into ν_s.[2]

Taking into account an implicit dependence of $E_{\rm res}$ on μ_x, we can solve (10) for $\mu_x(r,t)$, plug it into Eq. (1), and find the distribution function of sterile neutrinos $N_s(E,t)$.

III. RESULTS

A. Energy output in sterile neutrinos

The approach sketched in Sec. II allows us to calculate the energy spectra and the total energy emitted in the form of sterile neutrinos ν_s during the *first second* after the core bounce.[3] Our results are summarized in Fig. 1 (energy carried out as a function of sterile neutrino parameters). Figure 1 both summarizes the production within our fiducial model and demonstrates the level of uncertainties that we associate with such production (see explanation below). Section IV further discusses the uncertainties and how they influence our ability to constrain particle physics models.

We stress that Fig. 1 *does not correspond to any constraints on sterile neutrino parameters*. Given our current knowledge about SN explosions in general and about SN1987A in particular, it is impossible to determine

[2]Notice, that this expression was obtained without any assumption about the value of the chemical potential and is valid for the case of $\mu_x \gg T$ as well.

[3]After ~1 sec post-bounce the temperature of the area of intense resonance conversion ($r \simeq 10$–20 km) decreases significantly and the production of sterile neutrinos is essentially switched off. Note, that the temperature inside the core can still be high so this switch off may be less relevant for the collisional production.

what energy loss would be incompatible with existing scarce observations (see Sec. IV for discussion).

B. Qualitative explanation of the results

We start with outlining the results and explaining qualitatively the features of the contours in Fig. 1. The parameters of sterile neutrinos are constrained by estimating the amount of energy they may carry away (see Sec. IV for further details). This energy is a nonmonotonic function of mass. The higher is the mass, the higher is the resonance energy, $E_{\rm res}$, given by Eq. (4). This energy reaches $\mathcal{O}(100)$ MeV for $m_s \sim 30$ keV. For $E_{\rm res} \gg T_{\rm max}$ the population of neutrinos is exponentially suppressed, switching the sterile neutrino production off as m_s increases. For small masses of sterile neutrinos, they are copiously produced, but carry less energy "per particle". As the mixing angle decreases for the fixed mass, the conversion probability (5) decreases as well. As a result, the number of emitted sterile neutrinos drops, which explains why the contours close at small θ.

At large mixing angles the situation is different. The resonance region increases with the increase of θ_0 and eventually, becomes larger than the mean free path [cf. Eq. (1)]. This, again, destroys the resonance condition and conversion becomes nonefficient. This explains the upper boundary of the contours in Fig. 1.

Formally, the maximal energy that can be carried by sterile neutrinos in our fiducial model is $E_s^{\rm max} \approx 1.5 \times 10^{53}$ erg, comparable with the total energy output in active neutrinos, $E_{\nu_\alpha} \simeq 10^{53}$ erg (per flavor). Such sterile neutrinos would be a significant cooling agent, affecting the temperature profile and effectively shutting down their own production. This backreaction has not been taken into account in our work and therefore their treatment is not done self-consistently. Therefore the red contours in Fig. 1 are definitely an overestimation and are shown only for the indication of the effect. In order to properly account for sterile neutrinos with such a strong backreaction, one would need a detailed numeric study. Here our goal was to demonstrate, that the backreaction of lepton number production is still a significant effect. This comment is applicable also to other figures we present in the text.

C. Quantifying the uncertainties

The efficiency of the energy emission and, hence, our ability to set meaningful bounds on the sterile neutrino parameters is sensitive to the temperature in the postbounce core. This quantity is not known experimentally and can only be deduced from simulations. Unfortunately, there is a range of viable models of supernova explosion and they can provide quite different results regarding the parameters inside the supernova. This is discussed in more detail in Appendix A.

Here, in order to indicate the level of uncertainties we repeat our calculations in the model with the same temperature profile, suppressed in amplitude by 20%—a highly conservative estimate, as the uncertainty in temperatures can be much higher, see the comparison of temperature in two different simulations at Fig. 6. However, even these modifications can lead to significant changes in sterile neutrino energy production. Figure 2 shows several additional "slices" at $m_s = $ const that illustrates the dependence of our results on assumed inner temperature $T_{\rm max}$.

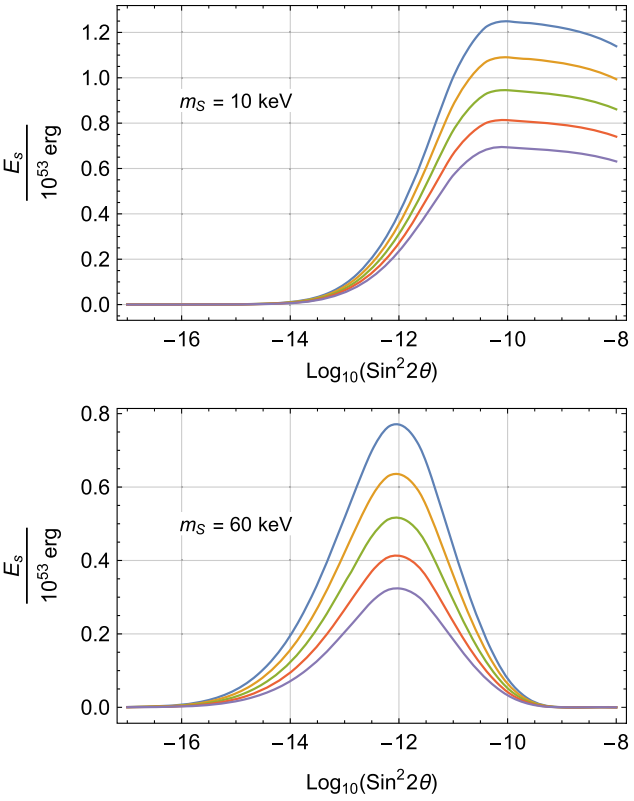

FIG. 2. Energy, emitted in the form of sterile neutrinos for fixed masses $m_s = 10$ keV (top plot) and 60 keV (bottom plot) depending on the mixing angle. Different contours correspond to temperature value modifier starting from 1 (fiducial model) that produces the largest energy output, to the set of values 0.95, 0.9, 0.85, and 0.8 as a sequence of contours with decreased production rate. We see that the model with ∼20% smaller $T_{\rm max}$ results in 3–4-times lower energy yield in sterile neutrinos.

D. The importance of diffusion

The solution of Eq. (10) allows to find the evolution of the chemical potential μ_x that governs the distribution of active antineutrinos. It is shown in Fig. 3. One sees that μ_x/T can reach significant values ($\mu_x \gtrsim T$).

To demonstrate the importance of backreaction effects we also studied two extreme scenarios: (i) the absence of diffusion and (ii) the absence of backreaction (infinite reservoir of neutrinos $\bar{\nu}_x$ at every energy and radius). In the former case the production $\bar{\nu}_x \to \nu_s$ stops very quickly, as the resonant conversion "consumes" all active antineutrinos

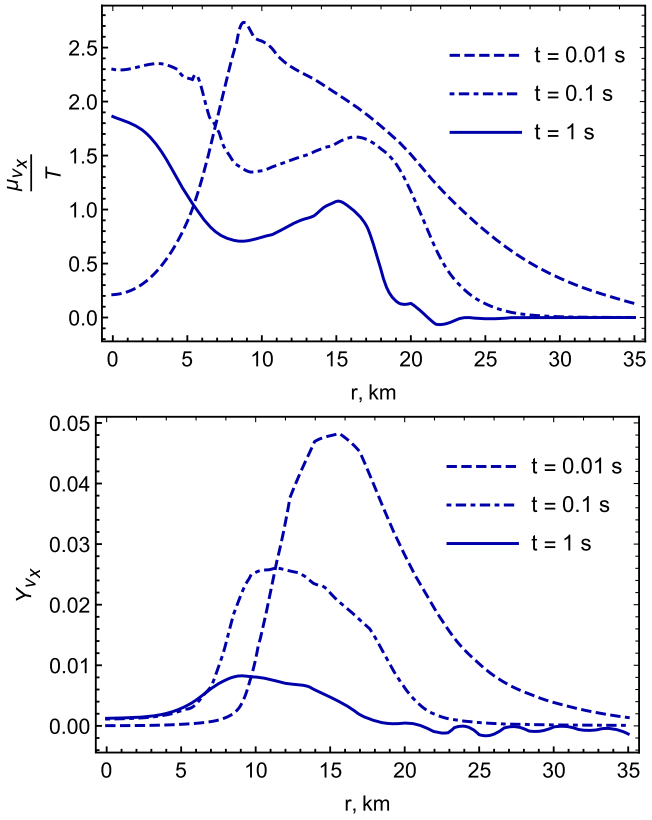

FIG. 3. Time evolution of the radial profiles of the chemical potential μ_τ and of the asymmetry parameter Y_τ in the fiducial model. Parameters of sterile neutrino are: mass $m_s = 7.1$ keV, the mixing angle $\sin^2 2\theta_\tau = 5 \times 10^{-11}$. The production of asymmetry starts at radii $r = 10$–20 km, and then diffuses both to the inner region, where it remains partially trapped, and to the outer regions, where it can be carried away via neutrino emission. Thus by $t \sim 1$ sec the chemical potential becomes negligible at $r \gtrsim 20$ km while still being nonzero in the core region due to the rapid decrease of the density of the SN and, hence, the increase of the neutrino diffusion rate at larger radii.

at a given radius and there are no mechanisms to replenish their population, as the large number of ν_x prevents the creation of $\nu_x\bar{\nu}_x$ pairs via Pauli blocking. (see also Appendix D for more details). Therefore the sizeable production of sterile neutrinos is possible in this case only for sufficiently large values of the mixing angle. In the case (ii), the population of antineutrinos $\bar{\nu}_x$ gets immediately restored and therefore the conversion rate remains the same throughout the whole time $t_{\rm pb} \sim 1$ sec, being extremely efficient. The production in the case (ii) stops only because neutrinos sufficiently cool down with the SN. It is this approximation that was used in [30] which explains higher total energy emitted in sterile neutrinos in their case. The realistic backreaction is in-between these two limiting cases, as Fig. 4 demonstrates.

The spectra of the resulting sterile neutrinos with different diffusion treatment are shown in Fig. 5.

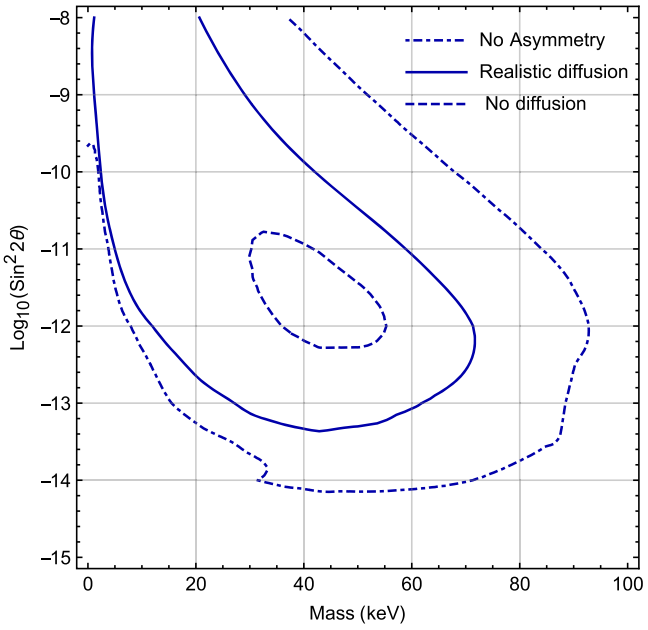

FIG. 4. Effects of the feedback. We show how energy contours ($E_s = 0.5 \times 10^{53}$ erg) changes for three different feedback mechanisms: the depleted lepton number is not repopulated by any means ("*no diffusion*" dashed line); the restoration of the lepton number proceeds much faster than sterile neutrino production ("*no asymmetry*" dashed-dotted line); and the case of the realistic diffusion, as studied in this work. The mixing is with ν_τ only and the duration of emission is taken to be 1 sec for all three cases.

E. Difference between muon and tau mixings

Although the presented mechanism works for both μ- and τ-mixing, the treatment of these two flavors differs, due to the fact that the temperature of the SN interior, as well as the value of the muon neutrino chemical potential μ_{ν_μ} (which appeared as a result of the backreaction), is high enough for muon pairs to be present (but not for tau leptons):

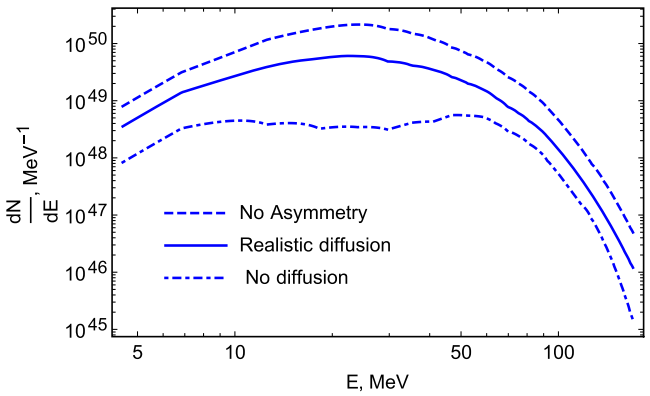

FIG. 5. Spectra of sterile neutrinos with mass $m = 7.1$ keV and the mixing angle $\sin^2 2\theta_x = 5 \times 10^{-11}$ produced during the first second of explosion for three cases of different backreactions from Fig. 4. Sterile neutrinos are mixed with τ-flavor.

$$\begin{aligned} Y_p &= Y_e + Y_\mu \\ \mu_e - \mu_{\nu_e} &= \mu_n - \mu_p = \hat{\mu} \\ \mu_\mu - \mu_{\nu_\mu} &= \mu_n - \mu_p = \hat{\mu} \end{aligned} \tag{11}$$

Once we fix SN-model dependent variables like total baryon density, the chemical potential of electrons, muon chemical potential can be calculated which will affect the neutrinos effective potential [Eq. (3)]. In the case of τ-leptons, their mass is too high even with nonzero μ_{ν_τ} to be produced. But even in the case of muon neutrinos production, the achieved $Y_\mu \ll 0.1$ hence does not affect the production at a noticeable level compared to tau-flavor mixing and there is no difference in the resulting amount of energy, carried by either flavor.[4] Therefore, our results (Fig. 1) does not depend on mixing flavor. We do not discuss here the influence of charged muons on the SN explosion [35].

F. Damping

The neutrino damping [34] describes the probability that a neutrino would interact with the medium while propagating in the resonance region. This interaction will cause the wave function to collapse to a pure flavor state, and its resonance conversion will become impossible. One can ignore the damping whenever $R_{\rm fwhm} \ll \lambda_{\rm mfp}$. In the opposite limit, the collisional production becomes important, as the scattering has a finite probability to leave behind not only pure active but also pure sterile state. The collisional production has been considered before in many works (see, e.g., Refs. [17,24,30,31]) and it is beyond the scope of the current work to study how it combines with the resonant production.

Its effect can be understood as follows: the width of the resonance $R_{\rm fwhm}$ is independent on the energy and proportional to the $\sin(2\theta_0)$ [Eq. (6)] while the mean free path of active neutrinos scales with energy as E^{-2} (see Sec. C 2). As a result for a given mass m_s and position $R_{\rm res}$ (equivalently *fixed resonance energy*) the ratio $R_{\rm fwhm}/\lambda_{\rm mfp}$ grows with θ_0. If one keeps the mixing angle (and $R_{\rm fwhm}$) fixed, but rather increases the mass—the resonance energy is increasing [Eq. (2)]. Therefore the mean free path of $\bar{\nu}_x$ decreases and neutrino damping becomes important.

G. Sterile neutrino as dark matter

So far we did not make any reference to sterile neutrinos being dark matter particles. The lifetime of sterile neutrinos lighter than two electron is given by (assuming for simplicity that θ_x is the only non-negligible mixing)

$$\tau_s \approx 2 \times 10^{24} \ \sec\left(\frac{10^{-11}}{\sin^2(2\theta_x)}\right)\left(\frac{20\ \text{keV}}{m_s}\right)^5 \tag{12}$$

—much longer than the lifetime of the Universe when $\theta^2 \sim 10^{-11}$. And indeed such particles represent a viable dark matter candidate (as suggested in [15,17,36–38], see [39] for a review).

We compute the energy output for a sterile neutrino with mass $m_s = 7.1$ keV and mixing angle $\sin^2 2\theta_x = (2-20)\times 10^{-11}$. Decay of such a sterile neutrino dark matter would produce an x-ray line, consistent with the observations of [32,33] and many subsequent works, see [39] for details. In this case, the energy output would be $E_s \approx 1.5 \times 10^{53}$ erg.

The gray shaded region in Fig. 1 shows the parameter space of the *neutrino minimal standard model* (νMSM) [40,41], see [42] for review where sterile neutrinos would have correct dark matter abundance (parts of this parameter space are excluded by x-ray and structure formation constraints, see [39] for review. The upper boundary corresponds to the parameters of the nonresonant dark matter production [17,36,38], while in the rest of the region the correct dark matter abundance can be obtained in the presence of primordial lepton asymmetry [17,37,43]. The maximal value of lepton asymmetry required to produce the correct dark matter abundance depends on the ratio of the mixing angles and differs, for example, in the model where $\theta_e = \theta_\mu = \theta_\tau$ as opposed to that with only $\theta_\tau \neq 0$ [43,44]. We conservatively chose to plot the lower bound corresponding to the maximal value of the lepton asymmetry attainable in the νMSM [42].

IV. DISCUSSION

In this paper, we analyzed the process of sterile neutrino creation during the explosion of a core-collapse supernova. Sterile neutrinos are produced via mixing with active antineutrinos of μ and/or τ flavors (collectively, $\bar{\nu}_x$). The hot and dense supernova environment is nontransparent for neutrinos and their dispersion changes as compared to the propagation in a vacuum. Therefore, the mixing with sterile neutrinos can become *resonant* (the MSW-like effect), leading to the effective conversion of antineutrinos $\bar{\nu}_x$ into sterile neutrinos with mass in the range $5\ \text{keV} \lesssim m_s \lesssim 40\ \text{keV}$ and mixing angles $\sin^2(2\theta_x)$ reaching 10^{-8} and below. The question of sterile neutrino production during supernovae explosion, their effects on explosion, and on the stellar nucleosynthesis has been studied in the past for sterile neutrinos ranging in masses from eV to GeV [9–30,45–47]. With few exceptions (e.g., Refs. [17,24,29,30]) these studies concentrated on the mixings of sterile neutrino with electron flavor. Recent work [30] argued that the fast production of sterile neutrinos is possible due to the MSW-like

[4] As the change in the effective potential and hence the resonance energy was too small.

resonance outside the SN core region when mixing with $\bar{\nu}_x$. However, the authors of [30] did not account for the depletion of the population of $\bar{\nu}_x$ in the resonance region and kept the distribution of active antineutrinos at its equilibrium level, thus providing a "stock" of antineutrinos to be converted. In reality, the depletion of the active antineutrinos slows down the conversion process; the $\nu_x - \bar{\nu}_x$ pair creation repopulates the abandoned states, and the above-equilibrium excess of ν_x gets diffused away.

In this work, we properly took into account the diffusion of the lepton number and the backreaction of sterile neutrinos on the neutrino distribution. Our results show that sterile neutrinos can carry away the amount of energy, comparable to that of active neutrino flavors (see Fig. 1). While the energy output can reach 10^{53} ergs—a ballpark figure associated with an SN explosion—*this does not lead to the bounds that are both strong and robust*.

Indeed, two main types of bounds from supernovae exist: *energy loss* and *energy-loss rate* bounds, see, e.g., Refs. [1–3,48]. The emission of any exotic component can be capped from above by $E_{\rm tot}$—the total energy available in an explosion. The latter is the difference between the binding energies of a progenitor and a remnant. The estimates of the total released energy $E_{\rm tot}$ depend on whether the remnant is a black hole or a neutron star. It is generally believed that the remnant of SN1987A is a neutron star, although the remnant has not been found [49] after more than 30 years of searches. The NS remnant can still be hidden behind SN debris [49,50] and there is a rising possibility that the remnant is indeed the NS according to recent work [51]. If the remnant is the neutron star, its binding energy can be estimated as

$$E_{\rm NS} \approx 6.3 \times 10^{53}\ {\rm erg} \left(\frac{\mathcal{C}}{0.6}\right) \left(\frac{M_{\rm NS}}{2\ M_\odot}\right)^2 \left(\frac{10\ {\rm km}}{R_{\rm NS}}\right) \quad (13)$$

with the coefficient $\mathcal{C} \approx 0.6$ [52–54]. The estimates put the mass for the SN1987A remnant in the range $M_{\rm NS} \simeq 1.7$–$1.9\ M_\odot$, see [49] for review. Alternative scenarios for a black hole formation in the SN1987A explosion exist [55–58]. In any case, the energy emitted in sterile neutrinos (Fig. 1) is smaller than $E_{\rm NS}$.

The energy loss rate argument [1–3] $\epsilon_{\rm extra} \lesssim 10^{53}$ erg/ sec is based on the shortening of the active neutrino signal duration in presence of additional cooling channel. The corresponding study was provided for the case of axions [59–61] and although there might be differences in details of production mechanisms (namely, the area of production in the case of the resonant neutrino production correspond mostly to regions, that are located outside the core and up to neutrinosphere while axions are produced the most intensively in the core), we can expect the same order-of-magnitude constraint. The same bound, of course, can be applied for sterile neutrinos, produce via scatterings [14,17,18,23,24].

In addition to the previous points, the output of sterile neutrinos is sensitive to the temperature (and temperature profile) in the inner regions of the SN. For $m_s \sim \mathcal{O}(1\ {\rm keV})$ the available neutrino population scales as $E_{\rm res}^2$ in the whole SN region where the condition $E_{\rm res}(R) \ll T$ holds. For $m_s \sim \mathcal{O}(100\,{\rm keV})$, since $E_{\rm res} \gg T$ everywhere, the number of "available" neutrinos scales exponentially with the inner temperature. The temperature dependence is thus more pronounced for the higher mass sterile neutrinos.

No observables are sensitive to the temperatures in these regions as the emission of active neutrinos happens from the outer regions—the neutrinosphere with $R_{\nu{\rm sph}} > R_{\rm res}$. Therefore, even detailed measurements of the neutrino fluxes would not tell us about the conditions under which sterile neutrinos were produced. Knowledge of the temperature profile (that would allow recovering $T(R_{\rm res})$ given the "measurement" of $T(R_{\nu{\rm sph}})$ can only be inferred from the simulations (similar to, e.g., Refs. [26,28] that however deal with heavier sterile neutrinos and/or different production mechanisms and influence on the SN dynamics). Such bonds will necessarily be model-dependent. We leave the self-consistent treatment of these cases to future works.

Finally, we note that the same challenges are faced by energy loss bounds applied to other hypothetical very weakly interacting particles: axions, dark photons, millicharged particles, etc.

ACKNOWLEDGMENTS

We would like to thank G. Fuller, G. Raffelt, I. Tamborra, I. Timiryasov, and Y.-Z. Qian for many useful discussions and comments on the draft. O. R. thanks the organizers of the *"Neutrino Quantum Kinetics in Dense Environments"* workshop for creating a stimulating environment. This work was supported by the Carlsberg Foundation and by the European Research Council (ERC) under the European Union's Horizon 2020 research and innovation Program No. (GA 694896).

Note added.—When this manuscript was finished, the paper [31] appeared that also investigates the production of ν_s mixed with ν_τ in the SN interior. Reference [31] analyzes the evolution of the lepton asymmetry Y_τ due to the resonance conversion and the collisional production as well as the feedback on the effective potential. The main difference for the resonance conversion study is that we

account for the neutrino's lepton number diffusion which eases the backreaction. Therefore our results are qualitatively similar, the difference can be attributed to different SN explosion models.

APPENDIX A: THE FIDUCIAL SUPERNOVA MODEL

The main goal of our paper is to demonstrate the effect of backreaction from the build-up of the lepton asymmetry on the resonant production of sterile neutrinos. The sterile neutrino emission depends on the spatial and temporal distribution of density of baryons ρ_B, temperature, asymmetries of electrons and of neutrinos Y_e, Y_{ν_α}. These quantities cannot be measured directly and in general require the numerical solution of a system of hydrodynamic transport equations to learn something about their properties. This introduces a number of systematic uncertainties.

Different numerical approaches to the supernova give broadly consistent results (see, e.g., the comparison of codes and approximations in [62,63]). Typical differences in various observables obtained with different codes are $\mathcal{O}(10\%)$. On the other hand, different assumptions about the SN progenitors can lead to very different temperature profiles (under otherwise equivalent assumptions), see example in Fig. 6.[5] The difference of $T_{\max}$ can lead to order-of-magnitude changes in the number of produced sterile neutrinos (see Appendix E) at fixed mass and mixing angle.

Another important uncertainty comes from the unknown equation of state (EoS) of nuclear matter. Different equations of state (see, e.g., Refs. [69–72]) appear as a result of different treatment of nuclear matter and its composition, see, e.g., Ref. [73]. The evolution of proto-neutron stars and corresponding neutrino signal under the assumption of different EoS were actively studied [74–82]. The nuclear equation of state can even be decisive in whether the simulation of an explosion would be successful [81–84]. Overall, depending on the nuclear equation of state, the parameters that are crucial for the production of sterile neutrinos—temperature, density, and lepton asymmetries—can vary significantly (see, for example, comparison of numeric results in [77,79]).

Given all these uncertainties, in this work, we purposely do not establish any constraints and demonstrate that the current state of the art (both observational and theoretical) does not allow us to provide any robust constraints.

However, in order to perform the analysis and estimates the magnitude of the described effects, we adopt a

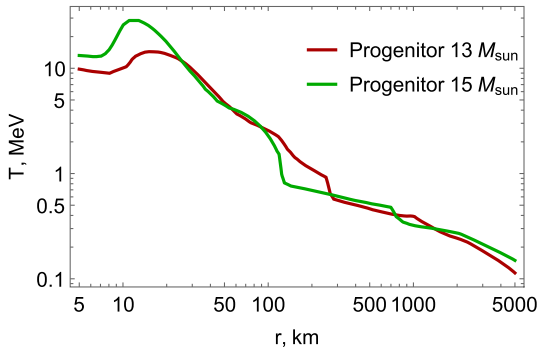

FIG. 6. Dependence of the temperature profiles (and in particular of the maximal temperature, $T_{\max}$) on the mass of progenitors. Both temperature profiles are for the same postbounce time $t_{pb} \simeq 250$ m sec and obtained as a result of simulations with the same numerical code [66]. The plots are shown for two different progenitor models with the main sequence masses of 13 $M_\odot$ [67] and 15 $M_\odot$ [68] that provided the initial conditions for the corresponding runs. The uncertainty in the determination of the mass of the progenitor of the SN1987A is 15–20 $M_\odot$ [see, e.g., Ref. [65]]. Although the selected time for a snapshot does not correspond to the period, when everything in the SN is settled down, we believe it perfectly demonstrates mentioned potential discrepancy in the SN media conditions during the explosion which can be relevant for the sterile neutrino production.

fiducial SN model, compute sterile neutrino production within it, and then quantify possible uncertainties. Our model is based on a 1D hydrodynamic simulation of an SN model [85] with the progenitor mass of 18.6 $M_\odot$ and SFHo nuclear equation of state [79] and the gravitational mass of 1.4 $M_\odot$. To allow for simplified analytical treatment of the problem, instead of using the exact temporal evolution of the SN background we use a model, when we have three snapshots for density, temperature and electron asymmetry profile obtained in simulation at post-bound times $t_{\rm pb} = 0.05$, 0.5, 1 sec (see Fig. 7). We use these parameters from snapshots as static background during the correspondent time intervals $(0 \le t < 0.05,\ 0.05 \le t < 0.5,\ 0.5 \le t < 1)$ and evolve the HNL production as well as μ/τ-asymmetry over this static background. So, for every new time interval, the initial profile of the lepton asymmetry is taken from the previous step evolution. While keeping the calculation as simple as for the completely static profile, this allows to follow the changes in production rate during different postbounce times.

Somewhat similar model and a similar approach have been recently used, e.g., in [31,86]. At times $t_{\rm pb} > 1$ sec, the temperature drops down to the values below few MeV, which results in a low rate of ν_s creation. That is why we do not take into account times $t > 1$ sec.

[5]The progenitor of the SN1987A is a blue supergiant star Sk − 62°202 [64] whose mass is estimated to be in the range 15–20 $M_\odot$ [65].

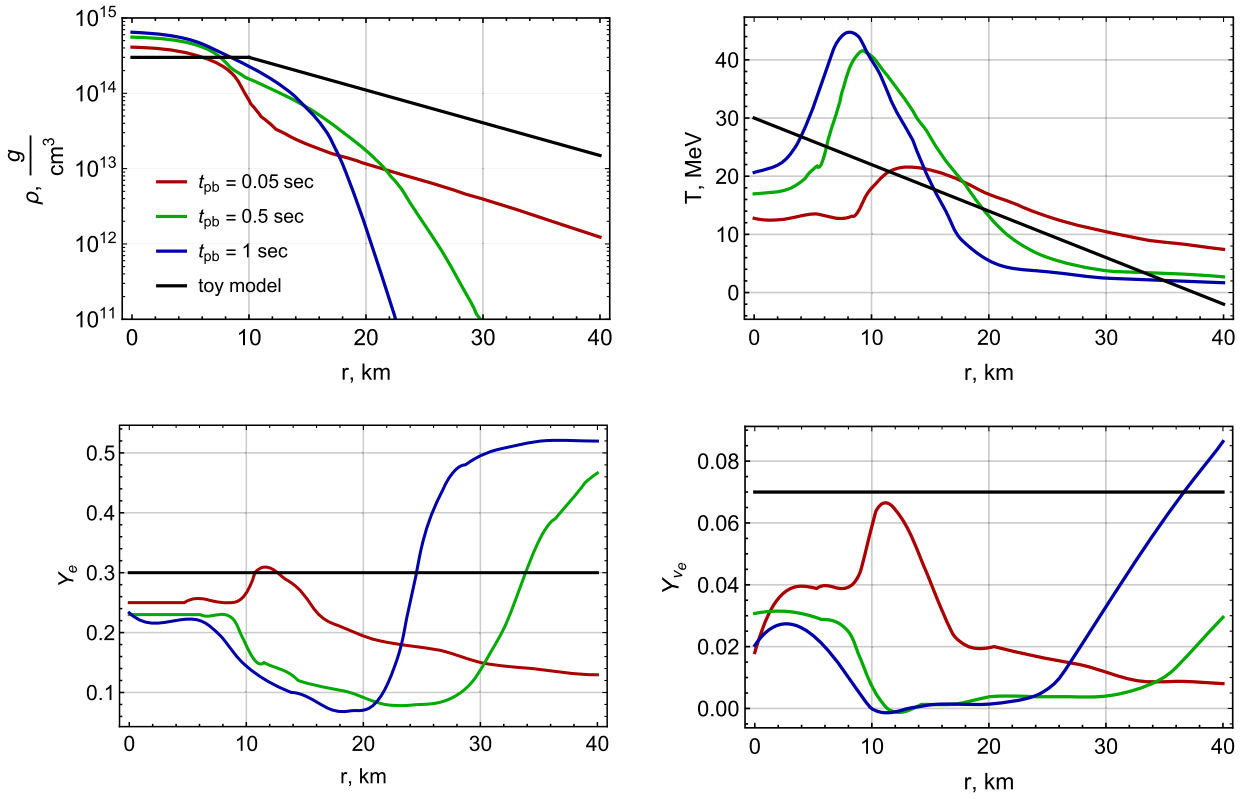

FIG. 7. Radial profiles of density, temperature, electron and electron neutrino asymmetries, taken as snapshots from 1D hydrodynamic simulations of the 18.6 $M_\odot$ supernovae explosion [85]. Postbounce times are $t_{pb} = 0.05$, 0.5, 1 sec. Black lines show the (time-independent) profiles in our toy model, used in Appendix E below.

APPENDIX B: RESONANT STERILE NEUTRINOS PRODUCTION

For completeness, we reproduce the formalism of the resonant conversion for neutrinos propagating in the media with changing density. Each of the flavor states $\nu_x, \bar{\nu}_x$ as well as ν_s obeys the Dirac equation and as a consequence the Klein-Gordon equation. When particles are ultrarelativistic in the medium of variable density this equation can be brought into the form (see, e.g., the book [Ref. [2] Chap. 8]):

$$i\frac{d}{dr}\begin{pmatrix}\bar{\nu}_x\\ \nu_s\end{pmatrix} = \mathcal{H}_{\rm eff}(r)\begin{pmatrix}\bar{\nu}_x\\ \nu_s\end{pmatrix} \tag{B1}$$

where the "effective Hamiltonian" is

$$\mathcal{H}_{\rm eff}(r) = \frac{m_s^2}{4E}\begin{pmatrix}-\cos 2\theta_0 & \sin 2\theta_0\\ -\sin 2\theta_0 & \cos 2\theta_0\end{pmatrix} + \begin{pmatrix}V_{\rm eff}(r) & 0\\ 0 & 0\end{pmatrix}. \tag{B2}$$

Here $V_{\rm eff}$ is the effective potential of $\bar{\nu}_x$ given by (see Eq. (3) for details/notations):

$$\begin{aligned} V_{\rm eff}(r) &= -\frac{G_F}{\sqrt{2}}N_{\rm b}(Y_n - 2Y_{\nu_e} - 2Y_{\nu_\tau} - 4Y_{\nu_\mu} - 2Y_\mu)\\ &= 11.4\ {\rm eV}\left(\frac{N_{\rm b}}{N_0}\right)(Y_n - 2Y_{\nu_e} - 2Y_{\nu_\tau} - 4Y_{\nu_\mu} - 2Y_\mu), \end{aligned} \tag{B3}$$

m_s is the mass of sterile neutrino, E is its energy ($m_s \ll E$) and we have neglected masses of the active neutrinos; θ_0 is the vacuum active-sterile mixing angle. The sign of $V_{\rm eff}$ is such that only the mixing $\bar{\nu}_x - \nu_s$ is relevant and therefore we have omitted ν_x state in Eq. (B1).

For future convenience we will introduce the notation

$$\Delta_s = \frac{m_s^2}{2E}. \tag{B4}$$

When $V_{\rm eff} = 0$ the eigenvalues of the Hamiltonian (B2) are $\pm\frac{1}{2}\Delta_s$ and the vacuum active-sterile oscillation length is given by π/Δ_s.

Notice that $[\mathcal{H}_{\rm eff}(r), \mathcal{H}_{\rm eff}(r')] \neq 0$ for $\theta_0 \neq 0$ and therefore exact solution of Eq. (B1) is complicated. For the propagation inside the star where $|\nabla \log V_{\rm eff}| \ll \Delta_s$ one can, however, solve this equation in the adiabatic limit.

To this end one diagonalizes (B2) at every point by the matrix $U(r)$, given by

$$U(r) = \begin{pmatrix} -\cos\theta(r) & \sin\theta(r) \\ -\sin\theta(r) & \cos\theta(r) \end{pmatrix} \tag{B5}$$

where the *matter mixing angle* $\theta(r)$ is defined (assuming $\theta_0 \ll 1$)

$$\tan 2\theta(r) \simeq 2\theta_0 \frac{\Delta_s}{\Delta_s + V_{\rm eff}(r)} + \mathcal{O}(\theta_0^2) \tag{B6}$$

From Eq. (B6) one sees that deep inside the SN, where $\Delta_s < |V_{\rm eff}(r_{\rm in})|$ and $V_{\rm eff} < 0$, one has $\tan 2\theta_{\rm in} \to -0 \Leftrightarrow \theta_{\rm in} \to \frac{\pi}{2}$, because θ is confined to $0 \le \theta \le \frac{\pi}{2}$. On the other hand, when the condition

$$\Delta_s + V_{\rm eff}(r) = 0 \tag{B7}$$

is satisfied, one has a resonance and $\theta_{\rm res} \to \frac{\pi}{4}$. Due to the sign of effective potential, resonance condition (B7) can be satisfied only for antineutrinos. Equation (B7) establishes a relation between the antineutrino energy and the radius of the resonance, $R_{\rm res}$:

$$V_{\rm eff}(R_{\rm res}) = -\frac{m_s^2}{2E} \tag{B8}$$

which leads to Eq. (2).

Diagonalization of the Hamiltonian (B2) gives two eigenvalues $E_{a,b}(r)$ such that

$$E_{a,b}(r) = \frac{V_{\rm eff}}{2} \pm \sqrt{(\Delta_s + V_{\rm eff})^2 + 4\Delta_s^2\theta_0^2} \tag{B9}$$

and two eigenfunctions (mass eigenstates) $\nu_{a,b}$. In the medium with variable density the states $\nu_{a,b}$ propagate according to the equation, similar to Eq. (B1):

$$i\frac{d}{dr}\begin{pmatrix} \nu_a \\ \nu_b \end{pmatrix} = \begin{pmatrix} E_a(r) & i\theta'(r) \\ -i\theta'(r) & E_b(r) \end{pmatrix}\begin{pmatrix} \nu_a \\ \nu_b \end{pmatrix} \tag{B10}$$

The off-diagonal elements in the r.h.s. are equal to $-iU^\dagger\partial_r U$ and are responsible for transition between different mass eigenstates that would be absent for $\theta' = 0$. Let us introduce a parameter of nonadiabaticity, γ

$$\gamma \equiv \frac{\theta'(r)}{E_a(r) - E_b(r)} \tag{B11}$$

Its value determines whether a transition between different levels is possible. When $\gamma \to 0$, the evolution is fully adiabatic and transitions between mass eigenstates are negligible (this is the case, for example, in the Sun). It turns out that for small θ_0 γ can be different from zero only in a narrow region around the resonance for a wide range of densities (effective potential) profiles (see Fig. 8). This is the region where the mixing angle changes its value significantly. Defining this region as where $\theta(r)$ changes from $\sin^2 2\theta = 1$ to $\sin^2 2\theta = \frac{1}{2}$ (i.e., $\frac{\pi}{8} \le \theta(r) \le \frac{3\pi}{8}$) we get its width $R_{\rm fwhm} = 2\sin(2\theta_0)/(\log V_{\rm eff}(R_{\rm res}))'$, Eq. (6). The nonadiabaticity parameter is maximal at the resonance and can be expressed through the width of the resonance

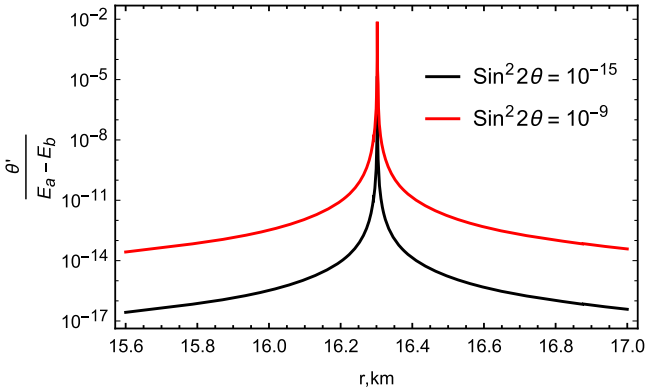

FIG. 8. Evolution with radius of the adiabaticity parameter $\gamma = \frac{\theta'}{E_a - E_b}$ [Eq. (B11)]. It can reach large values in a very narrow region around the resonance ($R_{\rm res} \simeq 16.3$ km in this case) and is extremely small outside it. The energy of the neutrino equals $E = 40$ MeV, sterile neutrino mass $m_s = 10$ keV. For smaller angle, the value of this parameter can be larger than 1. It shows that conversion goes nonadiabatically while for larger angle it acquire value $\ll 1$ everywhere, so the conversion is totally adiabatic.

$$\gamma = \frac{1}{\pi}\frac{L_{\rm osc}}{R_{\rm fwhm}} \tag{B12}$$

where $L_{\rm osc}$ is the oscillation length at resonance (7). The probability of transition between mass states ν_a and ν_b after crossing the resonance is given by [87]

$$P_{x\to s} = \frac{1}{2} - \left(\frac{1}{2} - P_{\rm na}\right)\cos 2\theta_{\rm in}\cos 2\theta_{\rm out}, \tag{B13}$$

where $\theta_{\rm in} \simeq \frac{\pi}{2}$—mixing angle, at the point of neutrino state creation and $\theta_{\rm out} = \theta(r_{\rm out}) \simeq \theta_0$—the vacuum mixing angle. $P_{\rm na}$ is a probability of transition between mass eigenstates due to nonadiabatic change of $V_{\rm eff}$. In the case, when $R_{\rm fwhm}$ is much smaller than the characteristic scale, over which $V_{\rm eff}$ is changing, the effective potential can be approximated as a linear function of $(r - R_{\rm res})$ around the resonance. In this case the Landau-Zener formula appears

$$P_{\rm na} = \exp\left[-\frac{\pi}{2\gamma}\right]. \tag{B14}$$

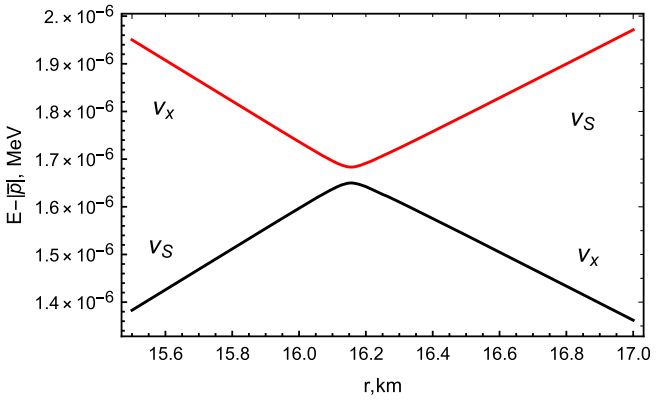

FIG. 9. Energy levels E_a (black), E_b (red) of the system, depending on the radius. Mixing angle is chosen as $\sin^2 2\theta = 10^{-3}$, mass $m_s = 10$ keV, momentum $p = 30$ MeV. The y-axis shows $m_{a,b}/2E$. The closest distance between energy levels is at the resonance where the transition between the levels is the most likely.

For small vacuum mixing angles one has $\theta_{\rm in} \approx \frac{\pi}{2}$ and $\theta_{\rm out} \approx \theta_0 \ll 1$, Eq. (B13) can be rewritten as

$$P_{x\to s} = 1 - \exp\left[-\frac{\pi}{2\gamma}\right]. \tag{B15}$$

Figure 9 illustrates the above considerations. Energy levels $E_a(r)$ and $E_b(r)$ do not cross. The value $E_a - E_b$ reaches its minimum as $r \to R_{\rm res}$. In the case of fully adiabatic propagation (i.e., change of the radius) one remains on the same energy level $E_a(r)$ or $E_b(r)$. As a result, a state $|\nu_x\rangle$ that is *mostly* $|\nu_a\rangle$ deep inside the star would remain *mostly* $|\nu_a\rangle$ everywhere and would exit the star as mostly sterile state $|\nu_s\rangle$. The probability of such a process for $\theta_0 \ll 1$ is given by $P^{\rm adiab}_{x\to s} \sim \cos^2\theta_0 \to 1$—the result familiar from the MSW effect in the Sun. This can be seen from Eq. (B15) when the parameter of nonadiabaticity $\gamma \to 0$.

The nondiagonal elements in the Hamiltonian make propagation nonadiabatic. Therefore, although levels do not cross, when they are approaching close to each other, a transition between them can occur. As a result, the probability for an active neutrino to pass a resonance region without conversion remains finite. One can consider the limit $\gamma \gg 1$, where the probability behaves as $P_{x\to s} \approx \frac{\pi}{2\gamma} = \frac{\pi^2}{2}\frac{R_{\rm fwhm}}{L_{\rm osc}} \ll 1$.

1. Mixing with the electron flavor

The described mechanism can of course be used for $\nu_e - \nu_s$ mixing as considered in a number of papers [9,12,45,46]. The effective potential for $\nu_e/\bar\nu_e$ is, however, different from (3):

$$V^{\nu_e,\bar\nu_e}_{\rm eff}(r) = \mp\frac{G_F}{\sqrt{2}} N_{\rm b}(-2Y_e + Y_n - 4Y_{\nu_e} - 2Y_{\nu_\tau} - 2Y_{\nu_\mu}). \tag{B16}$$

(the upper sign is for ν_e, the lower—for $\bar\nu_e$). Using the relations (11) one can see that the effective potential (B16) changes its sign as one moves away from the core. As a result, the production is possible for both electron neutrinos and antineutrinos. While the resonant conversion for $\bar\nu_e$ proceeds similarly to $\bar\nu_x$, for electron neutrinos the resonance condition is satisfied at two different radii. So ν_s converted at an inner radius can be reconverted to active neutrinos at an outer radius, reducing the effectiveness of the production (see, e.g., [Ref. [45] Fig. 3]). The kinetic equation (1) does not take this into account. Another important effect is that the value of Y_{ν_e} is tightly connected with the electron-positron asymmetry Y_e via beta-equilibrium condition. Therefore, efficient resonant conversion may shift beta-equilibrium and in this was significantly affect the nucleosynthesis in supernovae (see [88]). A proper self-consistent treatment of these processes are beyond the scope of this paper, therefore, we limit ourselves only to the mixing with μ and τ flavors.

APPENDIX C: BACKREACTION OF STERILE NEUTRINOS

1. Evolution of x-flavor population

The active-sterile conversion depletes the number of antineutrinos of given energy at a given radius [the two are related via Eq. (2)]. Therefore, the conversion could have led to the deviation of the $\bar\nu_x$ distribution function from its initial equilibrium form. However, other processes such as nucleon-neutrino scatterings

$$\bar\nu_x + N \to \bar\nu_x + N \tag{C1}$$

lead to the change of the shape of the antineutrino distribution function without changing the total number of antineutrinos at the radius r. The nucleon-nucleon bremsstrahlung production of neutrino pairs,

$$N + N \to N + N + \bar\nu_x + \nu_x, \tag{C2}$$

partially repopulates the number of $\bar\nu_x$ (without changing the total lepton number). The process (C2) is stopped by the *neutrino* Pauli blocking. The reaction rates of the processes (C1)–(C2) are faster than sterile neutrino conversion rate [89]. Therefore we can always describe the population of $\bar\nu_x$ by the equilibrium distribution function,

$$\bar f_x(E, r, t) = \frac{1}{(2\pi)^3}\frac{1}{\exp[\frac{E+\mu_x(r,t)}{T(r)}] + 1} \tag{C3}$$

(with $\mu_x \to -\mu_x$ for neutrino distribution function). *The evolution of the neutrino population is fully encoded into the evolution of the chemical potential* μ_x.[6]

The evolution of the chemical potential affects the effective potential $V_{\rm eff}$ and, therefore, the resonance energy (2) via the change of the lepton number Y_x. It can be seen from (2) that with the growth of Y_x the resonance energy increases so that the number density of active antineutrinos with energy $E \gtrsim E_{\rm res}$ diminishes and as a result the production stops.[7]

The nonzero chemical potential $\mu_x \sim T$ means that neutrino average energy increases. For the muon flavor large values of $\mu_x(r,t)$, increase the number of neutrinos that can participate in the production of muons in reactions, like

$$\nu_\mu + n \to p + \mu^- \tag{C4}$$

$$\nu_\mu + e^- \to \mu^- + \nu_e \tag{C5}$$

$$\nu_\mu + \bar{\nu}_e \to \mu^- + e^+ \tag{C6}$$

leading to the non-negligible population of μ^-. Similar reactions are possible for antineutrinos and antimuons, but the number density of $\bar{\nu}_\mu$ is extremely small in this regime, leading to negligible production of μ^+. So the muon lepton asymmetry will be stored not only in neutrinos but in muons as well. The population of $\tau^\pm$ leptons remains negligible because of their large mass.

2. Diffusion

The inhomogeneous chemical potential $\mu_x(r,t)$ triggers the lepton number diffusion processes. *Neutrinos* (whose number exceeds greatly that of antineutrinos) diffuse away and the reactions like (C2) then replenish population of antineutrinos.

A typical time scale for the diffusion over the distance R is $t_{\rm Diff} = \frac{R^2}{\lambda_{\rm mfp}}$, where $\lambda_{\rm mfp}$ is the mean free path of (anti) neutrinos of x-flavor. The neutrino's mean free path depends on the neutrino energy and matter density. A straightforward computation of neutrino scattering in a medium of nonrelativistic nucleons gives $\lambda_{\rm mfp} \sim \frac{\pi}{G_F^2 N_{\rm b} E^2}$.[8] Typical values of neutrino energies in supernovae is $E \sim \mathcal{O}(100)$ MeV and densities can reach $N_{\rm b} \sim 2 \times 10^{38}$ cm^{-3} so diffusion time can be as low as $\mathcal{O}(10^{-2}$ sec)—much below the period of time over which we analyse the sterile neutrino production. Therefore diffusion cannot be neglected. Strictly speaking, the diffusion approximation is not valid for $R \gtrsim R_{\nu{\rm sph}}$ where the density drops below $\rho < 10^{11}$ g/cm^3 and neutrinos start to free stream. The region of the neutrinosphere thus serves as a "sink" of lepton asymmetry. We can, however, ignore this correction thanks to the following consideration: (i) neutrinos are actively converted at $R_{\rm res} \ll R_{\nu{\rm sph}}$. (ii) The value of the lepton asymmetry at $R \gg R_{\rm res}$ does not influence directly this conversion rate because the diffusion rate at these "low" densities becomes very high ($t_{\rm Diff} \ll 1$ sec). As a result lepton asymmetry is washed out faster than it is produced. So it cannot accumulate and affect the value of the asymmetry in the inner region. To check these arguments we artificially increased the diffusion coefficient at $R \sim R_{\nu{\rm sph}}$ to effectively mimic free-streaming of neutrinos. The resulting asymmetry evolution appeared to be absolutely *identical* to the original scenario at a given accuracy. Therefore, no additional treatment for the lepton number inside the neutrinosphere is needed.

To describe the evolution of the lepton asymmetry we use (D2) with the diffusion coefficient $D(r,E)$ given by the relaxation time approximation:

$$D(r,E) = \frac{\lambda_{\rm mfp}(r,E)}{3} = \frac{\pi}{3 G_F^2 N_{\rm b}(r) E^2} \tag{C7}$$

(Appendix D).

The collisional production of sterile neutrinos can also affect the evolution of the chemical potential. Indeed, let $\Gamma^{\rm coll}_{\nu_x \to \nu_s}$ be the rate of collisional production of sterile neutrinos $\nu_x \to \nu_s$, while $\Gamma^{\rm coll}_{\bar{\nu}_x \to \nu_s}$ be a similar rate for antineutrino production (of course, ν_x and $\bar{\nu}_x$ produce sterile states of opposite helicity). Naively, one could argue that as there are more ν_x than $\bar{\nu}_x$ in the resonance region, the collisions will predominantly convert $\nu_x \to \nu_s$, thus decreasing the asymmetry. This is, however, not the case as the collision rates are not the same, $\Gamma^{\rm coll}_{\nu_x \to \nu_s} \ll \Gamma^{\rm coll}_{\bar{\nu}_x \to \nu_s}$ in the resonance region, see, e.g., Ref. [17] where the resonance enhancement/suppression of the collisional production rate is discussed. Indeed, the collision rates are proportional to $\sin^2(2\theta)$. In the resonance region, angle for antineutrinos is $\theta^{\bar{\nu}_x}_{\rm res} \sim \mathcal{O}(1)$, while for neutrinos $\theta^{\nu_x}_{\rm res} \simeq \frac{1}{2}\theta_0$, as one can see by replacing $V_{\rm eff} \to -V_{\rm eff}$ in Eq. (B6) and making use of the condition (B7). As a result

$$\Gamma^{\rm coll}_{\nu_x \to \nu_s} \sim \theta_0^2 \Gamma^{\rm coll}_{\bar{\nu}_x \to \nu_s} \tag{C8}$$

With chemical potential reaching $\mu_x/T \sim 3$ (see Fig. 3) $n_{\bar{\nu}_x} \sim 10^{-2} n_{\nu_x}$ and therefore we conclude that collisions do not contribute significantly to the wash out of lepton

[6]Recall that we only analyze the duration of time $t_{\rm pb} \sim 1$ sec and therefore neglect temporal change of the temperature profile.

[7]Sufficiently large asymmetry could cause the effective potential to change the sign and therefore cause conversion $\nu_x \to \nu_s$. Such a process would result in washing out of the asymmetry. We will see below that this does not happen for the realistic values of the parameters.

[8]Recall that we are interested only in the diffusion of μ or τ flavors and therefore only neutral current processes contribute to the scattering of both neutrinos and antineutrinos.

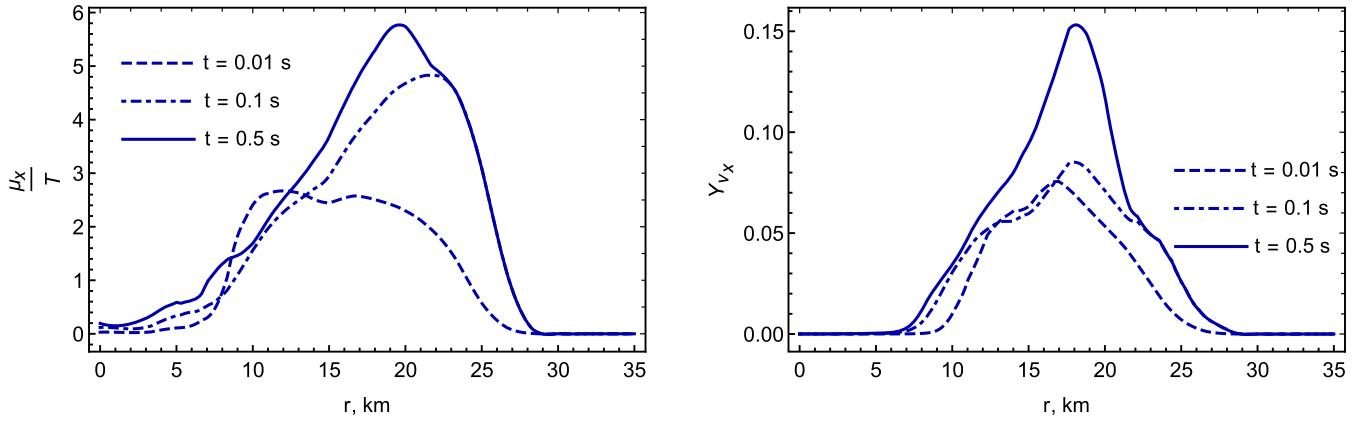

FIG. 10. The same as for Fig. 3, but without diffusion. In this case, asymmetry increases at every point independently. In the absence of diffusion the maximum asymmetry is sufficiently larger, but $V_{\rm eff}$ still does not change its sign. The peak position is changing slightly due to the change of resonance condition Eq. (2) with the build-up of the asymmetry Y as well as with the change of parameters of SN.

asymmetry for mixing angles that we are considering. Evolution of neutrino asymmetry without the diffusion is presented at Fig. 10.

3. Effects on the electron flavor population

As mentioned before, in the case of the mixing with ν_μ, the development of the chemical potential of the muon lepton number would lead to the asymmetry in charged muons. In its turn, this will affect electrons and electron neutrinos via the charge neutrality condition $Y_p = Y_e + Y_\mu$, changing the asymmetry of electrons. Connection between charged leptons and correspondent neutrinos is expressed with beta-equilibrium relations:

$$\mu_\mu - \mu_{\nu_\mu} = \mu_n - \mu_p = \hat{\mu} \tag{C9}$$

$$\mu_e - \mu_{\nu_e} = \mu_n - \mu_p = \hat{\mu} \tag{C10}$$

Charge neutrality and beta-equilibrium allow us to connect all these parameters of the supernovae medium. As a consequence of the increase of the muon neutrino chemical potential, we will have decreased values of electron density and density of ν_e. This effect, however, affects the overall results only marginally, as even with backreaction, muon neutrinos chemical potential (see Fig. 3).

APPENDIX D: LEPTON ASYMMETRY EVOLUTION

We start from radial diffusion equation for distribution function with a source

$$\frac{\partial f_x(r,E,t)}{\partial t} = \frac{1}{r^2}\frac{\partial}{\partial r}\left(r^2 D(r,E)\frac{\partial f_x(r,E,t)}{\partial r}\right) + I_x(r,E,t) \tag{D1}$$

where f_x is the distribution function of ν_x ($\bar{\nu}_x$), $D(E,r)$ is the diffusion coefficient, $I_x(r,E,t)$ is the source. By taking Eq. (D1) for neutrinos and antineutrinos, integrating their difference over momentum, and dividing by $N_{\rm b}$ we find:

$$\frac{\partial Y_x(r,t)}{\partial t} = \frac{1}{N_{\rm b}(r)}\frac{1}{r^2}\int \frac{\partial}{\partial r}\left(r^2 D(r,E)\frac{\partial}{\partial r}(f_x(E,r,t) - \bar{f}_x(E,r,t))\right)d^3p + S_x(r,t) \tag{D2}$$

here $S_x(r,t)$ is the integrated source of asymmetry

$$S_x(r,t) = \frac{\pi}{N_{\rm b}(r)} E^2_{\rm res}(r,t) f^{\bar{\rm out}}_x(E_{\rm res}(r),r,t) \times P_{x\to s}(E_{\rm res}(r),r,t)\frac{dE_{\rm res}}{dr}(r,t) \tag{D3}$$

Combining these results together, we arrive to the final equation describing the evolution of lepton number, Eq. (10).

APPENDIX E: QUANTIFYING THE UNCERTAINTIES

The production of sterile neutrinos is most sensitive to the maximum temperature in the SN as it defines the population of the highest-energy active neutrinos, that will be available for conversion. In order to quantify the uncertainties due to variation of different parameters, we adopt the toy model which has no temporal evolution. In this way, we can estimate the sensitivity of our results on the models not measured directly.

The baryon density is approximated as a constant inside the supernova core ($r < R_{\rm core}$) and decays exponentially at larger radii,

$$\rho_B = \rho_0 \exp\left[-\frac{r - R_{\rm core}}{R_{\rm core}}\right], \qquad r > R_{\rm core} \tag{E1}$$

TABLE I. Parameters of the toy model of the supernova adopted in this section. Temperature is chosen to decrease linearly from $T_{\max}$ at $r = 0$ to $T_{\min}$ at $r = 50$ km and is also constant during the first second. See Appendix A for other details.

Core radius	$R_{\text{core}} = 10$ km
Maximum temperature	$T_{\max} = 30$ MeV
Minimum temperature	$T_{\min} = 3$ MeV
Baryon core density	$\rho_0 = 3 \times 10^{14} \frac{\text{g}}{\text{cm}^3}$
Baryon core number density	$N_0 = 10^{38}$ cm^{-3}
Proton fraction	$Y_p = 0.3$

Temperature is chosen to decrease linearly from $T_{\max}$ at $r = 0$ to $T_{\min}$ at $r = 50$ km and is also constant during the first second. Proton number fraction remains constant and it is just a simplification for our model (note that does not necessarily mean that we define the number of electrons as there may be a change of population of other charge massive leptons). Numerical values of the relevant parameters are specified in Table I.

Comparison with the simulation snapshots (Fig. 2) shows, that the values of asymmetries are on the same order of value, while density decreases slower and temperature can be both higher, and lower, than in the fiducial model but is, again of the same order. So, our toy model serves as a fair representation of the realistic profile.

We see, that although the parameters of the SN in specific regions differ significantly (at the outer radii $r \gtrsim$ 20–30 km for density and inner radii $r \simeq 10$ km for temperature), the maximum total energy outcome has not changed significantly. This happens due to a very strong backreaction that localizes the production to a compact spatial region in the interior of the neutron star.

In order to quantify the uncertainties, The change of energy outcome with temperature decrease is also of the same order (while the temperature modification has also a similar factor of 15%–20%). It shows, that uncertainty of the result due to exact temperature inside supernovae was not a feature of the specific model we used. The results for emitted energy for toy model and for small variations of temperature within it are presented at Fig. 11.

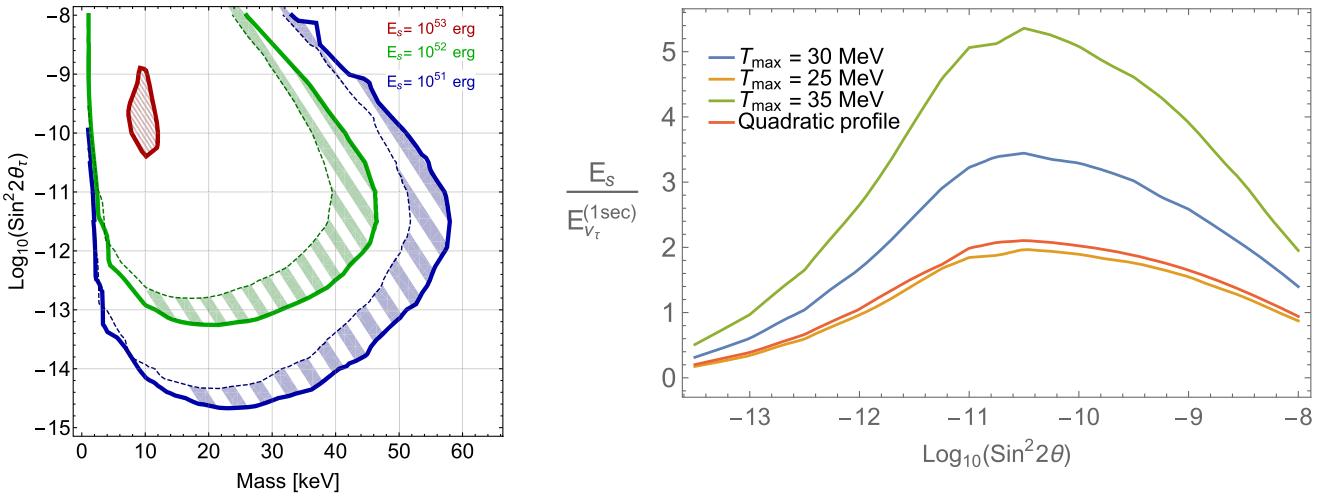

FIG. 11. Left panel: energy emitted by sterile neutrinos in toy model (thick lines) and modified toy model of Sec. E (thin dashed lines) —when central temperature in the SN is decreased to 25 MeV, which correspond to scaling of temperature for ≈15%. Shaded region shows the corresponding "uncertainty" of production. Sterile neutrino are considered mixed solely with ν_τ. Right panel: uncertainties related to the SN temperature models. Energy, emitted in the form of sterile neutrinos as a function of the mixing angle for the mass $m_s = 20$ keV. The curves show the effects of changing the maximal temperature $T_{\max}$ by ± 5 MeV as well as and different scaling of the temperature profile between $T_{\max}$ and $T_{\min}$ (quadratic rather than linear).

[1] G. G. Raffelt, Phys. Rep. **198**, 1 (1990).
[2] G. G. Raffelt, *Stars as Laboratories for Fundamental Physics* (Chicago University Press, USA, 1996), p. 664.
[3] G. G. Raffelt, Annu. Rev. Nucl. Part. Sci. **49**, 163 (1999).
[4] R. Essig *et al.*, in *Proceedings, 2013 Community Summer Study on the Future of U.S. Particle Physics: Snowmass on the Mississippi (CSS2013): Minneapolis, MN, USA, 2013* (2013), arXiv:1311.0029.
[5] S. Alekhin *et al.*, Rep. Prog. Phys. **79**, 124201 (2016).
[6] D. Notzold and G. Raffelt, Nucl. Phys. **B307**, 924 (1988).
[7] L. Wolfenstein, Phys. Rev. D **17**, 2369 (1978).
[8] S. P. Mikheev and A. Yu. Smirnov, Yad. Fiz. **42**, 1441 (1985) [, Sov. J. Nucl. Phys. **42**, 913 (1985)].
[9] K. Kainulainen, J. Maalampi, and J. T. Peltoniemi, Nucl. Phys. **B358**, 435 (1991).
[10] G. Raffelt and G. Sigl, Astropart. Phys. **1**, 165 (1993).
[11] J. T. Peltoniemi, Astron. Astrophys. **254**, 121 (1992).
[12] X. Shi and G. Sigl, Phys. Lett. B **323**, 360 (1994); **324**, 516 (E) (1994).
[13] A. Kusenko and G. Segre, Phys. Lett. B **396**, 197 (1997).
[14] A. D. Dolgov, S. H. Hansen, G. Raffelt, and D. V. Semikoz, Nucl. Phys. **B580**, 331 (2000).
[15] A. D. Dolgov and S. H. Hansen, Astropart. Phys. **16**, 339 (2002).
[16] A. D. Dolgov, S. H. Hansen, G. Raffelt, and D. V. Semikoz, Nucl. Phys. **B590**, 562 (2000).
[17] K. Abazajian, G. M. Fuller, and M. Patel, Phys. Rev. D **64**, 023501 (2001).
[18] G. M. Fuller, A. Kusenko, I. Mocioiu, and S. Pascoli, Phys. Rev. D **68**, 103002 (2003).
[19] M. Barkovich, J. C. D'Olivo, and R. Montemayor, Phys. Rev. D **70**, 043005 (2004).
[20] J. Hidaka and G. M. Fuller, Phys. Rev. D **74**, 125015 (2006).
[21] J. Hidaka and G. M. Fuller, Phys. Rev. D **76**, 083516 (2007).
[22] A. Kusenko, B. P. Mandal, and A. Mukherjee, Phys. Rev. D **77**, 123009 (2008).
[23] G. M. Fuller, A. Kusenko, and K. Petraki, Phys. Lett. B **670**, 281 (2009).
[24] G. G. Raffelt and S. Zhou, Phys. Rev. D **83**, 093014 (2011).
[25] M.-R. Wu, T. Fischer, L. Huther, G. Martínez-Pinedo, and Y.-Z. Qian, Phys. Rev. D **89**, 061303 (2014).
[26] M. L. Warren, M. Meixner, G. Mathews, J. Hidaka, and T. Kajino, Phys. Rev. D **90**, 103007 (2014).
[27] M. Warren, G. J. Mathews, M. Meixner, J. Hidaka, and T. Kajino, Int. J. Mod. Phys. A **31**, 1650137 (2016).
[28] T. Rembiasz, M. Obergaulinger, M. Masip, M. A. Pérez-Garcia, M.-A. Aloy, and C. Albertus, Phys. Rev. D **98**, 103010 (2018).
[29] S. Zhou, Int. J. Mod. Phys. A **30**, 1530033 (2015).
[30] C. A. Argüelles, V. Brdar, and J. Kopp, Phys. Rev. D **99**, 043012 (2019).
[31] A. M. Suliga, I. Tamborra, and M.-R. Wu, J. Cosmol. Astropart. Phys. 12 (2019) 019.
[32] A. Boyarsky, O. Ruchayskiy, D. Iakubovskyi, and J. Franse, Phys. Rev. Lett. **113**, 251301 (2014).
[33] E. Bulbul, M. Markevitch, A. Foster, R. K. Smith, M. Loewenstein, and S. W. Randall, Astrophys. J. **789**, 13 (2014).
[34] L. Stodolsky, Phys. Rev. D **36**, 2273 (1987).
[35] R. Bollig, H. T. Janka, A. Lohs, G. Martinez-Pinedo, C. J. Horowitz, and T. Melson, Phys. Rev. Lett. **119**, 242702 (2017).
[36] S. Dodelson and L. M. Widrow, Phys. Rev. Lett. **72**, 17 (1994).
[37] X.-D. Shi and G. M. Fuller, Phys. Rev. Lett. **82**, 2832 (1999).
[38] T. Asaka, M. Laine, and M. Shaposhnikov, J. High Energy Phys. 01 (2007) 091. , 02 (2015) 028.
[39] A. Boyarsky, M. Drewes, T. Lasserre, S. Mertens, and O. Ruchayskiy, Prog. Part. Nucl. Phys. **104**, 1 (2019).
[40] T. Asaka and M. Shaposhnikov, Phys. Lett. B **620**, 17 (2005).
[41] T. Asaka, S. Blanchet, and M. Shaposhnikov, Phys. Lett. B **631**, 151 (2005).
[42] A. Boyarsky, O. Ruchayskiy, and M. Shaposhnikov, Annu. Rev. Nucl. Part. Sci. **59**, 191 (2009).
[43] M. Shaposhnikov, J. High Energy Phys. 08 (2008) 008.
[44] J. Ghiglieri and M. Laine, J. High Energy Phys. 11 (2015) 171.
[45] H. Nunokawa, J. T. Peltoniemi, A. Rossi, and J. W. F. Valle, Phys. Rev. D **56**, 1704 (1997).
[46] I. Tamborra, G. G. Raffelt, L. Hudepohl, and H.-T. Janka, J. Cosmol. Astropart. Phys. 01 (2012) 013.
[47] Z. Xiong, M.-R. Wu, and Y.-Z. Qian, Astrophys. J. **880**, 81 (2019).
[48] R. Adhikari *et al.*, J. Cosmol. Astropart. Phys. 01 (2017) 025.
[49] D. Alp *et al.*, Astrophys. J. **864**, 174 (2018).
[50] P. Esposito, N. Rea, D. Lazzati, M. Matsuura, R. Perna, and J. A. Pons, Astrophys. J. **857**, 58 (2018).
[51] D. Page, M. V. Beznogov, I. Garibay, J. M. Lattimer, M. Prakash, and H.-T. Janka, Astrophys. J. **898**, 125 (2020).
[52] J. M. Lattimer and M. Prakash, Astrophys. J. **550**, 426 (2001).
[53] J. M. Lattimer, eConf **C0507252**, L007 (2005).
[54] H.-T. Janka, Neutrino emission from supernovae, in Handbook of Supernovae, edited by A. W. Alsabti and P. Murdin (Springer International Publishing AG, Cham, Switzerland, 2017), p. 1575.
[55] G. E. Brown, S. W. Bruenn, and J. C. Wheeler, Comments Astrophys. **16**, 153 (1992).
[56] J. F. Beacom, R. N. Boyd, and A. Mezzacappa, Phys. Rev. D **63**, 073011 (2001).
[57] K. Blum and D. Kushnir, Astrophys. J. **828**, 31 (2016).
[58] N. Bar, K. Blum, and G. D'Amico, Phys. Rev. D **101**, 123025 (2020).
[59] A. Burrows, M. S. Turner, and R. P. Brinkmann, Phys. Rev. D **39**, 1020 (1989).
[60] W. Keil, H.-T. Janka, D. N. Schramm, G. Sigl, M. S. Turner, and J. R. Ellis, Phys. Rev. D **56**, 2419 (1997).
[61] T. Fischer, S. Chakraborty, M. Giannotti, A. Mirizzi, A. Payez, and A. Ringwald, Phys. Rev. D **94**, 085012 (2016).
[62] O. Just, R. Bollig, H.-T. Janka, M. Obergaulinger, R. Glas, and S. Nagataki, Mon. Not. R. Astron. Soc. **481**, 4786 (2018).
[63] E. O'Connor *et al.*, J. Phys. G **45**, 104001 (2018).
[64] R. Gilmozzi, A. Cassatella, J. Clavel, C. Fransson, R. Gonzalez, C. Gry, N. Panagia, A. Talavera, and W. Wamsteker, Nature (London) **328**, 318 (1987).

[65] A. Weiss, Astrophys. J. **339**, 365 (1989).
[66] M. Liebendoerfer, M. Rampp, H. T. Janka, and A. Mezzacappa, Astrophys. J. **620**, 840 (2005).
[67] K. Nomoto and M. Hashimoto, Phys. Rep. **163**, 13 (1988).
[68] S. E. Woosley and T. A. Weaver, Astrophys. J. Suppl. Ser. **101**, 181 (1995).
[69] H. Shen, H. Toki, K. Oyamatsu, and K. Sumiyoshi, Nucl. Phys. **A637**, 435 (1998).
[70] G. Shen, C. J. Horowitz, and S. Teige, Phys. Rev. C **83**, 035802 (2011).
[71] J. M. Lattimer and F. D. Swesty, Nucl. Phys. **A535**, 331 (1991).
[72] M. Hempel and J. Schaffner-Bielich, Nucl. Phys. **A837**, 210 (2010).
[73] J. A. Pons, S. Reddy, P. J. Ellis, M. Prakash, and J. M. Lattimer, Phys. Rev. C **62**, 035803 (2000).
[74] S. Reddy, J. Pons, M. Prakash, and J. M. Lattimer, in Proceeding s of the 26th International Workshop on Gross Properties of Nuclei and Nuclear Excitation: Nuclear Astrophysics (Hirschegg 98) (1998), arXiv:astro-ph/9802310.
[75] M. Prakash, J. M. Lattimer, J. A. Pons, A. W. Steiner, and S. Reddy, Lect. Notes Phys. **578**, 364 (2001).
[76] J. A. Pons, S. Reddy, M. Prakash, J. M. Lattimer, and J. A. Miralles, Astrophys. J. **513**, 780 (1999).
[77] M. Prakash, I. Bombaci, M. Prakash, P. J. Ellis, J. M. Lattimer, and R. Knorren, Phys. Rep. **280**, 1 (1997).
[78] M. Hempel, M. Oertel, S. Typel, and T. Klähn, J. Phys. Soc. Jpn. Conf. Proc. **14**, 010802 (2017).
[79] A. W. Steiner, M. Hempel, and T. Fischer, Astrophys. J. **774**, 17 (2013).
[80] S. Reddy, M. Prakash, and J. M. Lattimer, Phys. Rev. D **58**, 013009 (1998).
[81] K. Sumiyoshi, S. Yamada, H. Suzuki, and S. Chiba, Phys. Rev. Lett. **97**, 091101 (2006).
[82] K. Sumiyoshi, S. Yamada, and H. Suzuki, Astrophys. J. **688**, 1176 (2008).
[83] E. O'Connor and C. D. Ott, Astrophys. J. **730**, 70 (2011).
[84] T. Fischer, M.-R. Wu, B. Wehmeyer, N.-U. F. Bastian, G. Martínez-Pinedo, and F.-K. Thielemann, Astrophys. J. **894**, 9 (2020).
[85] The Garching Core-Collapse Supernova Archive, https://wwwmpa.mpa-garching.mpg.de/ccsnarchive.
[86] A. M. Suliga, I. Tamborra, and M.-R. Wu, J. Cosmol. Astropart. Phys. 08 (2020) 018.
[87] S. J. Parke, Phys. Rev. Lett. **57**, 1275 (1986).
[88] J. Bliss, M. Witt, A. Arcones, F. Montes, and J. Pereira, Astrophys. J. **855**, 135 (2018).
[89] T. A. Thompson, A. Burrows, and J. E. Horvath, Phys. Rev. C **62**, 035802 (2000).